
Article:
Zare Pakzad, Sina, Nasr Esfahani, Mohammad orcid.org/0000-0002-6973-2205 and Alaca, B. Erdem (2023) The role of native oxide on the mechanical behavior of silicon nonowires. Materials Today Communications. 105002. ISSN 2352-4928

https://doi.org/10.1016/j.mtcomm.2022.105002

The Role of Native Oxide on the Mechanical Behavior of Silicon Nanowires

Sina Zare Pakzad[a], Mohammad Nasr Esfahani[b], B. Erdem Alaca[a,c,d,*]

[a]*Department of Mechanical Engineering, Koç University, Rumelifeneri Yolu, 34450 Sariyer, Istanbul, Turkey*
[b]*School of Physics, Engineering and Technology, University of York, York, YO10 5DD, UK*
[c]*n²STAR-Koç University Nanofabrication and Nanocharacterization Center for Scientific and Technological Advanced Research, Koç University, Rumelifeneri Yolu, 34450 Sariyer, Istanbul, Turkey*
[d]*Koç University Surface Technologies Research Center (KUYTAM), Koç University, 34450 Sariyer, Istanbul, Turkey*

Abstract

Molecular dynamics simulations are employed to study the effect of native oxide on the size-dependent mechanical properties of silicon nanowires. Despite their immense potential as essential building blocks in nanoelectromechanical systems, mechanical behavior of silicon nanowires still needs further attention for a full understanding. The leading source of ambiguity can be traced back to the fact that the presence of native oxide on silicon nanowire surfaces is ignored when interpreting nanomechanical test data, when it comes, for example, to converting force and deflection measurements to stress and strain. This problem needs immediate attention, because, first, nanowires have a significant surface area, and second, native oxide is the dominant surface state. With prior work reporting conflicting dimensional and computational viewpoints regarding the effect of native oxide on silicon nanowires properties, size dependence of nanowire mechanical properties is investigated here with great attention placed on critical size and atomistic simulation perspectives. For this purpose, Tersoff-Munetoh and modified Stillinger-Weber potentials are employed in this intensive computational study to address the influence of size and crystal orientation on nanowire elastic behavior and tensile strength. As a result, a striking set of differences is obtained. First, the presence of native oxide layer is observed to decrease both the modulus of elasticity and the ultimate strength. The reduction in the modulus of elasticity is observed

to be as much as 30% and 40% for $< 100 >$ and $< 110 >$-oriented nanowires, respectively. Similarly, the reduction in the ultimate strength is estimated to be as much as 20% using the modified Stillinger-Weber potential, which proved to be more suitable for strength analysis compared to Tersoff-Munetoh potential. Finally, the failure behavior is studied through the ductile failure probability calculations, where a higher size-dependent failure probability is observed for decreasing nanowire width upon oxidation. These results shed light on the background of existing inconsistencies between experimental and numerical findings in the literature, as opposing trends for silicon nanowire stiffness and strength were reported with decreasing size. The study provides a guideline to quantify the scale effect in silicon nanowire mechanical behavior as a combined outcome of oxide thickness, nanowire size and crystal orientation and thus to reduce the extent of uncertainties originating from inadequate interpretation of nanomechanical test data.

Keywords: Silicon nanowire, molecular dynamics, tensile behavior, native oxide, elastic modulus, strength

1. Introduction

Among the low-dimensional nanoscale materials that increasingly find applications in high-performance devices of diverse nature, nanowires (NWs) and nanotubes are of particular interest due to their utilization in the fields of electronics, energy harvesting and storage, sensing and communications [1, 2, 3, 4, 5, 6]. In the specific case of silicon (Si) NWs, this trend is fueled by a multitude of applications ranging from gate-all-around transistors [7, 8] to next-generation mass spectrometers [9, 10] with the latter representing a nanoelectromechanical system (NEMS) [11]. Such NEMS devices entail the potential of extreme miniaturization of today's sensors. Demonstrated by a series of exploratory studies [12, 13, 14], this miniaturization brings about the benefits of improved sensitivity and power consumption in sensor applications. Due to its ease of integration with electronics, maturity of fabrication technologies, and well-understood transduction via piezoresistivity, Si remains in the forefront of the miniaturization effort [2, 4]. As Si NWs

*Corresponding author
Email address: ealaca@ku.edu.tr (B. Erdem Alaca)

serve as the core mechanical building block in NEMS applications, a solid understanding of the scale effect on the mechanical properties is an inherent part in NEMS design and implementation. However, it is also the very scale that poses significant challenges for NW characterization [4, 15].

These challenges take different forms in experimental and modeling studies. In mechanical characterization experiments, physical requirements for reliable testing, such as alignment of the Si NW sample with respect to loading axis and imposing suitable boundary conditions are very stringent [16]. Various testing techniques including bending, uniaxial loading, indentation, and resonance address certain aspects of these requirements with varying levels of success [4, 5, 17]. In addition to the issues related to the mechanical nature of testing, challenges due to processing and metrology — sample preparation, device calibration and setup resolution in addition to the extraordinary challenges of *in-situ* characterization — contribute to the fact that the resulting spread in measurements remains significant. As a result, Si NW strength below the critical dimension of 400 nm is currently reported to cover several orders of magnitude ranging from 100 MPa up to 21 GPa, the theoretical strength of the crystal [4, 5, 15]. On the other hand, theoretical approaches including molecular dynamics (MD) simulations, *ab initio* and first-principal methods [4, 2] are very powerful techniques to study the mechanical properties using the force fields. In a similar fashion, such efforts also result in a wide range of estimations of Si NW mechanical properties [4]. This can be predominantly attributed to an inconsistent use of constitutive models for the study of surface bond reconstruction and nonlinearity in elasticity [4, 5, 2], and thus deserves a closer scrutiny.

Size-dependent mechanical properties of Si NWs have been modeled by MD simulations considering primarily parameters such as the NW diameter [18, 19, 20, 21, 22, 23] and its geometrical shape [24, 25, 26]. Surface-related properties of NWs were also addressed [21, 24] taking surface stress [27] and side surface crystalline orientations [28] into account. In addition to atomic simulations, continuum formulation was employed as well to address size dependence [4, 27]. However, most studies – both MD and continuum – considered the unreconstructed and passivated Si NW surfaces [29, 22, 30, 31, 32] while studying surface stress [27] and surface elasticity [33], thereby ignoring the presence of the native oxide as the primary surface structure [34, 35, 36, 37]. This native oxide layer, known to be amorphous silicon dioxide ($aSiO_2$) [38, 39], affects the local structure through creating interfaces and introducing defects [40, 41, 42]. This becomes especially significant at

the nanoscale, where minuscule variations in the oxide thickness and shape can lead to major changes in Si NW properties [43, 44, 45, 46, 47, 48, 49]. Despite the degree to which the native oxide is expected to affect Si NW mechanical behavior, to our knowledge, very limited work has been reported so far. For example, the existence of a compressive stress near the $aSiO_2$/Si interface was demonstrated in Si NWs [50] which can alter the surface stress state due to surface reconstruction. Another study on bending properties of oxidized Si NWs reported the reduction in NW stiffness due to the oxide layer when compared with pure Si NWs [49]. More recently, the effect of the native oxide was investigated via MD tensile modeling, where the effective modulus of elasticity and fracture strength were reported to decrease with increasing oxide thickness [51, 46]. Furthermore, predicting a negligible size effect in the case of Si nanocantilevers, findings of such theoretical studies remain in stark contrast with those of experimental investigations [44, 52]. In addition to the surface state, such disagreement between theory and experiment can also be linked to the specific interatomic potential used in MD simulations [25]. There are numerous interatomic potentials developed for Si and oxygen (O) including the Tersoff-Munetoh [53], Stillinger-Weber (SW) [54, 55], modified SW [56], and Vashishta [57] potentials. Similar to the elastic behavior, size-dependent brittle-to-ductile transition and orientation-dependent failure of Si NWs were previously studied using various interatomic models [29, 20, 58, 59, 21]. In this regard, there are studies putting forward both the slip mechanism [26, 60] and the crystal-to-amorphous phase transition [61, 62] as the source of ductility.

It is against this background that the present work is concerned with the mechanical behavior of Si NWs with a native oxide surface layer. MD simulations are used to model Si NW tensile behavior with an unreconstructed surface and native oxide using the Tersoff- Munetoh [53] and modified SW [56] potentials. The impact of the native oxide on the modulus of elasticity, yield and ultimate strength is studied in $< 100 >$ and $< 110 >$, the two most relevant crystallographic orientations found in top-down fabrication of Si NWs [4]. Furthermore, due to expected rectangular/square geometry of NWs upon top-down fabrication, the selection of the cross-sections are decided to be square opposite to circular cross-sections commonly encountered in $< 111 >$ oriented Si NWs as outcome of bottom-up fabrication attempts [4, 63]. In the remainder of this paper, details of the interatomic potentials and simulation methods are discussed first. This is followed by a case study on the native oxide effect on two different orientations with varying

interatomic potential, oxide thickness and NW length-to-width ratio. Furthermore, the analytical approach based on the core-shell model is employed for the comparison with MD results. The paper is concluded with a study on the orientation and interatomic-potential-dependent failure behavior in the presence of native oxide.

2. Materials and Methods

In this section, first the description of methods used to perform atomistic study on tensile behavior of Si NWs with and without native oxide is given. This includes geometrical definition and interatomic potentials used in this study. This is followed by the details of the analytic model, utilized for the estimation of the effective modulus of elasticity of NWs. MD simulations are employed to study the impact of native oxide on the tensile behavior of Si NWs. NWs with native oxide are denoted as $aSiO_2$-Si NWs throughout the rest of this work. Si NWs with unreconstructed surfaces are simply denoted as Si NWs. MD simulations are carried out on Si NWs along $< 100 >$ and $< 110 >$ crystal orientations using LAMMPS [64]. The initial configurations of Si NWs and $aSiO_2$-Si NWs are schematically shown in Figure 1. Periodic boundary conditions (B.C.s) were applied along x-direction, while applying fixed boundary condition along y- and z-directions to model a part of an infinite NW. The interaction between atoms in Si NWs and $aSiO_2$-Si NWs are modeled by the Tersoff-Munetoh [53] (TM), and modified SW [56] (m-SW) potentials. The details of the corresponding expressions and coefficients of the formulations for the TM and m-SW potentials can be found in the associated references. [53, 56] Figure 1 shows the geometrical definitions of the NW including width (W), oxide thickness (t), and length (L) while the length-to-width (L/W) ratio is denoted as the aspect ratio (AR). MD simulations are performed at a temperature of 10 K to obtain a quasi-static system. An initial velocity with a Gaussian distribution was assigned at a temperature of 10 K. This was followed by the energy minimization using the conjugate gradient method as a static relaxation. This energy minimization removes any excessive stress in the atomic structure for the dynamic equilibrium step. Then the structure was dynamically equilibrated at 10 K for 60 ps using the Nose-Hoover isobaric-isothermal (NPT) ensemble with a time step of 1 fs. After the equilibration, the simulation cell was deformed along the NW longitudinal direction with a strain rate of $\dot{\epsilon} = 5 \times 10^9 s^{-1}$, which is in the range of strain rates suitable for tensile tests in MD simulations. [29]

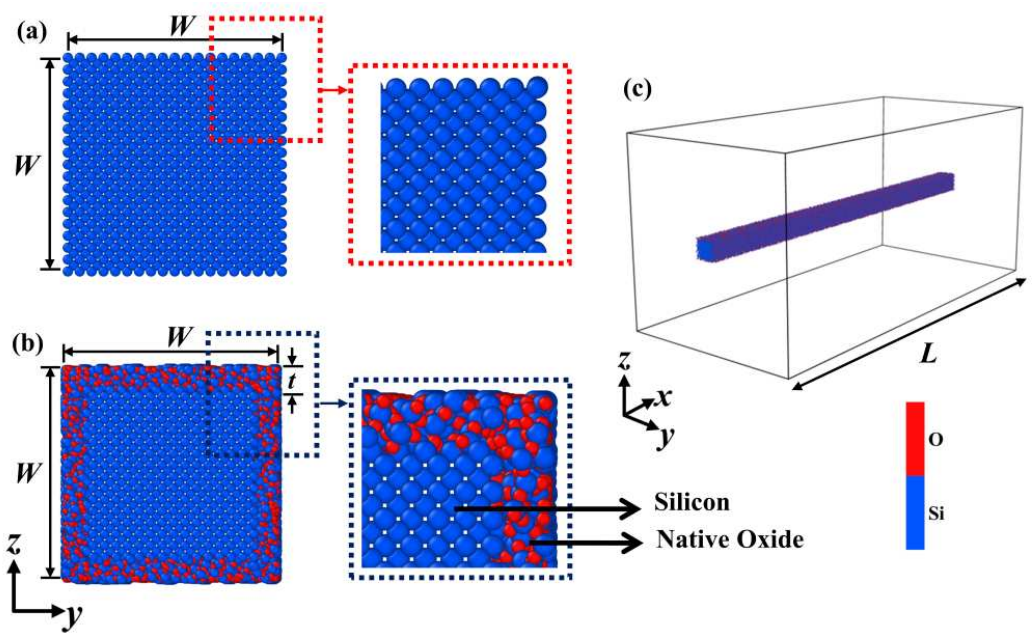

Figure 1: Cross-sections of models for (a) Si NWs and (b) $aSiO_2$-Si NWs studied here where surface condition of NWs are represented with close-ups. Si and O atoms are shown with blue and red spheres respectively. (c) The simulation box with a representative $aSiO_2$-Si NW with periodic B.C. applied along the NW direction (x) and non-periodic B.C.s applied along two other directions (y-direction and z-direction). Dimensional parameters defining NW sizes as width (W), length (L) and native oxide thickness (t) are shown here.

For a quasistatic system with negligible thermal oscillations, atomic stress based on the virial theorem [65] can be written as:

$$\pi_{ij} = \frac{1}{2\Omega_0}\Big[\sum_{\alpha=1}^{N}\sum_{\beta\neq\alpha}^{N}\frac{1}{r^{\alpha\beta}}\frac{\partial V(r^{\alpha\beta})}{\partial r}(v_i^{\alpha\beta}v_j^{\alpha\beta})\Big] \tag{1}$$

where Ω_0 stands for the atomic volume in an undeformed system with N as the total number of atoms. Atomic distances between atoms α and β are represented as $r^{\alpha\beta}$. v_j^{α} stands for the position of atom α along j direction, *i.e.* $v_j^{\alpha\beta} = v_j^{\alpha} - v_j^{\beta}$ and V represents the interatomic potential. The virial stress can be computed as a sum over all atoms (and atom pairs) in the simulation cell and then divided by the cell volume, *i.e.* the volume of the NW in this work.

The structure of $aSiO_2$-Si NWs can be considered as an $aSiO_2$ layer encap-

sulating a crystalline Si core. Hence, the core-shell model can be utilized as the basic approach to implement the surface effect on the elastic response. The core-shell model describes the NW as a combination of a core and a surface region with a distinct set of elastic properties. Considering a finite thickness of t for the surface layer, the modulus of elasticity of the NW, E, under tensile load is given in Eqn. 2 where the moduli of elasticity of bulk Si and $aSiO_2$ are denoted by E_{Si} and E_{aSiO_2}, respectively [66, 67].

$$E = E_{Si}[1 + 4(\frac{E_{aSiO_2}}{E_{Si}} - 1)(\frac{t}{W} - \frac{t^2}{W^2})] \tag{2}$$

Although the core-shell models are capable of considering the surface effect, a close estimation of E_{aSiO_2} and t are required. In this work, E_{Si} and E_{aSiO_2} are computed via tensile MD simulations, while Eqn. 2 is used for the estimation of the accuracy and trends of NW tensile simulation results. To estimate E_{Si} and E_{aSiO_2}, tensile tests are performed with the TM and m-SW potentials using periodic boundary conditions in all directions. Thus, the effect of native oxide on the mechanical behavior of Si NWs is studied using both MD and analytical models.

3. Results and Discussion

The influence of native oxide on the mechanical properties of Si NWs will be presented in this section through studying i) modulus of elasticity, ii) ultimate strength, and iii) fracture behavior. Results will be presented in the following sequence:

• In the first step, the reliability of interatomic potentials is studied for Si NWs and $aSiO_2$-Si NWs of the same size.

• Then, the effect of oxide thickness and AR is investigated using TM and m-SW interatomic potentials.

• Next, a comparison with the core-shell model is carried out to evaluate limits associated with using analytical methods to estimate the modulus of elasticity.

• Then the impact of the native oxide on the ultimate strength of Si NWs is studied based on both potentials.

• This is followed by a benchmark study on the role of crystal orientation on the performance of interatomic potentials.

• At the end of this section, the failure behavior of $aSiO_2$-Si NWs is compared to that of Si NWs.

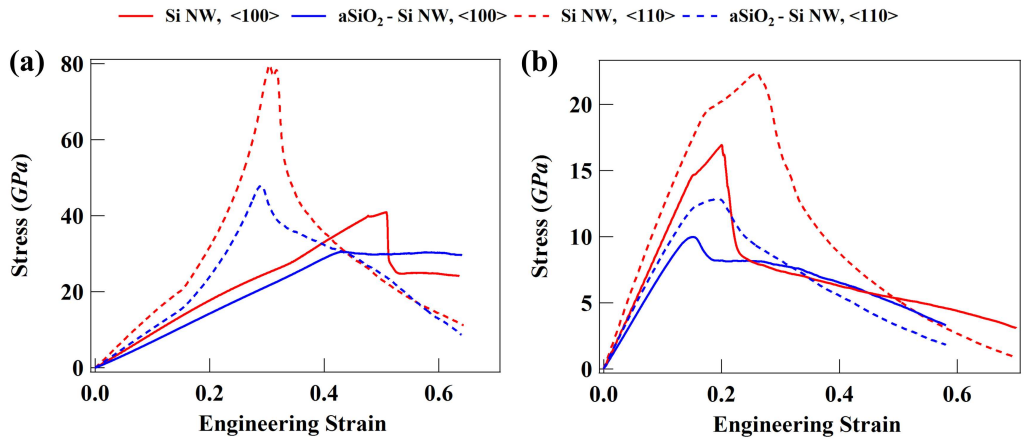

Figure 2: Stress-strain curves of Si NWs and $aSiO_2$-Si NWs modeled using the (a) TM, and (b) m-SW potentials. The associated orientations of Si crystal in NWs as $< 100 >$-Si and $< 110 >$-Si are depicted with solid and dashed lines, respectively. The corresponding change in stress-strain curves of Si NWs with native oxide (blue curves) compared to Si NWs with unreconstructed surface (red curves) exhibit the change in modulus of elasticity (slope of stress strain curve at strains <4%) and ultimate strength (maximum stress) of NWs due to presence of native oxide.

For a comparison of the TM and m-SW interatomic models, the mechanical properties of NWs are studied with $L = 100\ nm$, $W = 5\ nm$, and $t = 0.5\ nm$. Figure 2 depicts the stress-strain curves for Si NWs and $aSiO_2$-Si NWs modeled with both potentials. For small strains, the stress-strain relation is linear representing the elastic regime for all NWs, where the modulus of elasticity can be directly estimated. The stress then changes non-linearly reaching the ultimate strength. Beyond this point, and accompanied by necking, it decreases until fracture. The modulus of elasticity and ultimate strength measured from the stress-strain curves for Si NWs and $aSiO_2$-Si NWs are summarized in Table 1. Results show a reduction in the modulus of elasticity of $aSiO_2$-Si NWs compared to that of Si NWs. This change is about 25% and 30% for NWs along $< 100 >$ and $< 110 >$ crystal orientations, respectively.

The yield stress and strain analysis are performed by defining the starting point of deviation of the stress-strain curves from the linear curve with the slope of the predicted modulus of elasticity below 4% strain. The linear regime associated with stress-strain curves used for the modulus of elasticity estimations is given in Supplementary S.3. The stress-strain curves for NWs

Table 1: Modulus of elasticity and ultimate strength values calculated using different interatomic potentials for Si NWs and $aSiO_2$-Si NWs.

NW	Potential	Modulus of Elasticity (GPa)	Ultimate Strength (GPa)
Si $< 100 >$	TM	85.6	41.0
$aSiO_2$-Si $< 100 >$		63.4	30.6
Si $< 110 >$		145.8	79.4
$aSiO_2$-Si $< 110 >$		101.6	47.8
Si $< 100 >$	m-SW	97.1	16.9
$aSiO_2$-Si $< 100 >$		73.0	15.3
Si $< 110 >$		128.4	22.3
$aSiO_2$-Si $< 110 >$		91.7	14.8

modeled with the TM potential in Figure 2(a) show a linear increase up to a yield strain of 7.5% for Si NWs, whereas such deformation is limited to 4% for $aSiO_2$-Si NWs. Such yield analysis shows a decrease in the yield strength from 5.6 GPa and 11.6 GPa for Si NWs to 2.5 GPa and 5.8 GPa for $aSiO_2$-Si NWs in $< 100 >$ and $< 110 >$, respectively. A similar inspection with the m-SW potential demonstrated in Figure 2(b) shows a yield strain and a yield strength of 10% and 9.7 GPa decrease to 5.5% and 5.0 GPa upon oxidation, respectively. Exploration of yield strain and strength for $< 110 >$-oriented Si NW and $aSiO_2$-Si NWs using the m-SW potential indicates a similar reduction from 8% and 10.3 GPa to 5% and 4.9 GPa, respectively.

In the non-linear region of the stress-strain plots in Figure 2, a reduction in Si NW ultimate strength is observed for both crystal orientations. A decrease of 33% and 21% is obtained with the TM and m-SW potentials, respectively. Regardless of the surface state, there is a significant difference between the TM and m-SW potentials in predicting the ultimate strength. The reliability of these two potentials can be studied through comparing Figure 2 with experimental studies [4, 17, 15, 2]. The ultimate strength reported in experimental observations ranges between 10 GPa up to 23 GPa [4], where the ultimate strength predicted for $aSiO_2$-Si NWs modeled by the m-SW potential is in a similar range. In contrast, the TM potential overestimates the ultimate strength which can be linked to the soft cut-off scheme in the Tersoff potential [68, 69, 84]. Despite similarities of stress-strain curves obtained via both interatomic potentials for strains < 0.1, the overestimation of strength using the TM potential is reflected in results shown in Supplementary S.2.

This overestimation in the TM potential can be linked to the cut-off distance considered in the empirical model [68, 70, 71]. With prior examples of failure strength overprediction observed at nanoscale modelling efforts, it should be noted that recent MD simulations with Tersoff and Tersoff-like potentials would estimate the fracture strength and strain due to the problem of the cut-off function [68]. Further discussion and details on the discrepancies between the TM and m-SW potentials to predict the mechanical properties is provided in Supplementary S.2. Despite this challenge, the TM potential will be still used to study the native oxide effect on the mechanical behavior of NWs, considering that the TM potential is capable to accurately model the modulus of elasticity reduction due to the native oxide effect. Previously reported modulus of elasticity for Si NWs by experimental efforts [4, 17] is in the range of 65 GPa up to 230 GPa, comparable with the estimated modulus of elasticity for $aSiO_2$-Si NWs using the TM and mod-SW potentials as summarized in Table 1. Considering the deficiency of the TM potential to model the ultimate strength values, comparison of the fracture behavior with experimental work [4] will be carried out via m-SW potential only. A similar reduction in the mechanical properties of Si NWs with amorphous silica layer was reported previously [46]. As discussed earlier, the strain rate considered here is in the same range as those of previous MD studies of NW tensile tests [29]. The impact of the strain rate on the modeling of Si and $aSiO_2$-Si NWs NW tensile properties by the TM and m-SW potentials is presented in Supplementary S.1. The findings exhibit an almost negligible change of the modulus of elasticity and ultimate strength.

Having studied the performance of interatomic potentials, the impact of t on the mechanical properties of Si NWs is studied next. The native oxide thickness depends on parameters such as the crystallographic orientation and surface preparation [72]. Previous theoretical studies report a native oxide thickness ranging between 0.2 nm to 1.0 nm [46]. However, the oxide can be as thick as 2.0 nm using thermal oxidation processes [73]. To understand the influence of native oxide on the elastic behavior, at first, the effect of t is investigated for various AR. Tensile tests are carried out on NWs with $W = 5$ nm to 9 nm and $t = 0.5$ nm and 1.0 nm.

Figure 3 shows the modulus of elasticity according to the TM and m-SW potentials. Results generally exhibit a negligible dependence of the modulus of elasticity on AR for both surface states. The only considerable increase in the modulus of elasticity is observed for $aSiO_2$-Si NWs with $W = 6$ nm, if AR < 15. Further examination of the results in Figure 3 reveals a signif-

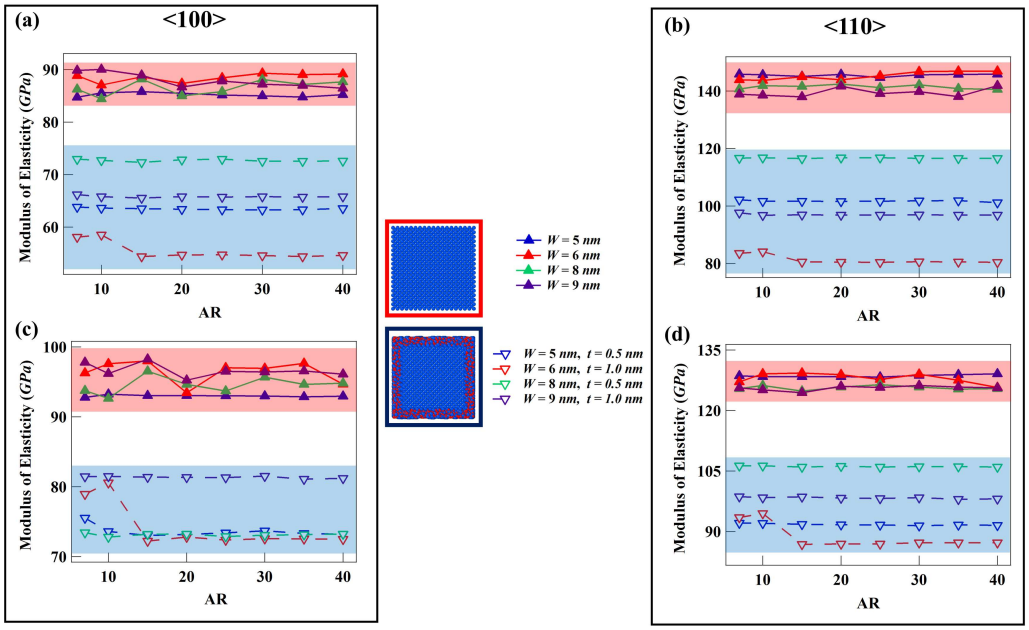

Figure 3: The modulus of elasticity as a function of AR for Si NWs and $aSiO_2$-Si NWs along (a) $< 100 >$ and (b) $< 110 >$ crystal orientations modeled by the TM potential and along (c) $< 100 >$ and (d) $< 110 >$ crystal orientations modeled by the m-SW potential. Different widths (and different native oxide thicknesses for $aSiO_2$-Si NWs) of NWs are examined where Si NWs and $aSiO_2$-Si NWs are color-coded with red and blue color codes on modulus of elasticity vs. AR graphs with different levels of reduction due to combined effects of size, native oxide thickness, crystalline orientation, and interatomic potential effects.

icant reduction of modulus of elasticity with increasing t, a direct result of the native oxide. However, the size effect on the modulus of elasticity for Si NWs remains insignificant in both crystal orientations. In addition, there is a size-dependent elastic response in $aSiO_2$-Si NWs, where increasing W at a constant t, increases the modulus of elasticity. This size effect becomes negligible in $aSiO_2$-Si NWs of $< 100 >$ modeled by the m-SW potentials, which can be traced back to the combined effect of W, crystal orientation and interatomic potential.

In addition to the interatomic potential, crystal orientation has a drastic impact on the modulus of elasticity. As discussed earlier in the context of native oxide effect on modulus of elasticity of Si NWs, the results in Figure 3(b) and Figure 3(d) also confirm that native oxide reduces the modulus of elasticity for $< 110 >$-oriented $aSiO_2$-Si NWs in a range of 15% to 42%,

Table 2: Modulus of elasticity of the bulk, E_{Si} and E_{aSiO_2}.

Material	Potential	Modulus of Elasticity of the Bulk (GPa)
Si $< 100 >$	TM	87.4
Si $< 110 >$		133.1
$aSiO_2$		59.4
Si $< 100 >$	m-SW	94.1
Si $< 110 >$		120.3
$aSiO_2$		111.7

depending on W and t. This change on the modulus of elasticity as a result of native oxide is in a range of 12% to 32% for $< 100 >$ NWs as shown in Figure 3(a) and Figure 3(c). This observation indicates that the native oxide effect on the elastic behavior in $< 110 >$ is stronger compared to $< 100 >$. This can be linked to a larger difference between the elastic moduli of $aSiO_2$ and Si $< 110 >$ compared to Si along $< 100 >$. The comparison of the modulus of elasticity for Si NWs and $aSiO_2$-Si NWs exhibits a drastic effect of the native oxide on NWs with smaller W. For instance, the reduction in modulus of elasticity observed for $aSiO_2$-Si NWs of W of 5 nm and 6 nm is more significant compared to W of 8 nm and 9 nm.

In the next step, an analytical model, *i.e.* the core-shell model, is used to verify the impact of the native oxide on the size-dependent elastic behavior of Si NWs. For this purpose, E_{Si} and E_{aSiO_2} of Eqn. 2 are predicted using MD simulations and are listed in Table 2. These results are in good agreement with previous theoretical and MD studies [49, 74] as well as experimental measurements [75]. A modulus of elasticity around 70-75 GPa was reported previously [76, 77, 78, 79, 80, 81] for $aSiO_2$, while in this study the TM potential predicts a lower E_{aSiO_2} compared to the m-SW potential as shown in Table 2. To examine the native oxide effect on the modulus of elasticity by the core-shell model, different oxide thicknesses are considered for $aSiO_2$-Si NWs as shown in Figure 4. Starting from the TM potential, the modulus of elasticity of NWs of $< 100 >$ modeled by MD changes from 70 GPa to 55 GPa with t increasing from 0.25 nm to 1.0 nm, while the core-shell model predicts a reduction from 80 GPa to 70 GPa. Similarly, the modulus of elasticity of $< 110 >$ NWs decreases with increasing t using both MD and core-shell methods, while some deviation between the predictions is observed. This discrepancy between MD simulations and the core-shell

model increases in the case of the m-SW potential, where MD simulations predict a change from 80 GPa to 70 GPa in contrast to the core-shell model estimating an almost constant E of 100 GPa. A similar difference between MD simulations and core-shell model is observed in $< 110 >$ NWs as well. MD results show a reduction in E from 105 GPa to 85 GPa by changing t from 0.25 nm to 1.0 nm, while the core-shell model estimates an almost constant E of 120 GPa. Stress-strain curves associated with each modulus of elasticity estimation depicted in Figure 4 are presented in Supplementary S.2. A previous MD study on the oxide effect in Si NWs reported a similar reduction in E with increasing t [46]. Despite such differences between modulus of elasticity predictions using MD and core-shell model, both methods clearly confirm the reduction due to the native oxide effect in $aSiO_2$-Si NWs. The difference between the predictions of the modulus of elasticity by the core-shell model and MD can be traced back to the non-continuous elasticity definition in core-shell model at the interface of bulk core Si and surface shell oxide regions. Such general assumption in core-shell model violates the continuity condition at the interface of the two layers and leads to unphysical interpretations of NW elastic response. To address this shortcoming, alternative approaches such as the modified core-shell models were proposed [82, 33]. Similarly, core-shell model also falls short of considering intrinsic effects such as stresses generated due to the formation of native oxide on NW surfaces with recent studies revealing stresses up to 2 GPa induced in Si NWs as a direct outcome of native oxide formation [83].

As the next stage, the TM and m-SW potentials are used to study the effect of native oxide on the ultimate strength of Si NWs and $aSiO_2$-Si NWs. The case of AR = 20 was already discussed in connection with Table 1. Figure 5 now depicts the ultimate strength as a function of AR. First of all, results regularly exhibit reduction of strength with oxidation. This reduction is in the range of 5% to 40% in the case of $< 100 >$-oriented $aSiO_2$-Si NWs, depending on W, t and interatomic potential, as shown in Figure 5(a) and Figure 5(c). For $< 110 >$, the reduction in strength is between 29% to 42% as depicted in Figure 5(b) and Figure 5(d). The amount of reduction in the ultimate strength for $aSiO_2$-Si NWs of $< 110 >$ is higher compared to NWs of $< 100 >$. This could be traced back to the differences between the ultimate strengths of core crystals compared to the native oxide. Analyzing the impact of t on the ultimate strength of $aSiO_2$-Si NWs as a function of AR reveals a decreasing ultimate strength of $aSiO_2$-Si NWs with increasing t. The SW potential predicts a raise in the ultimate strength with increasing

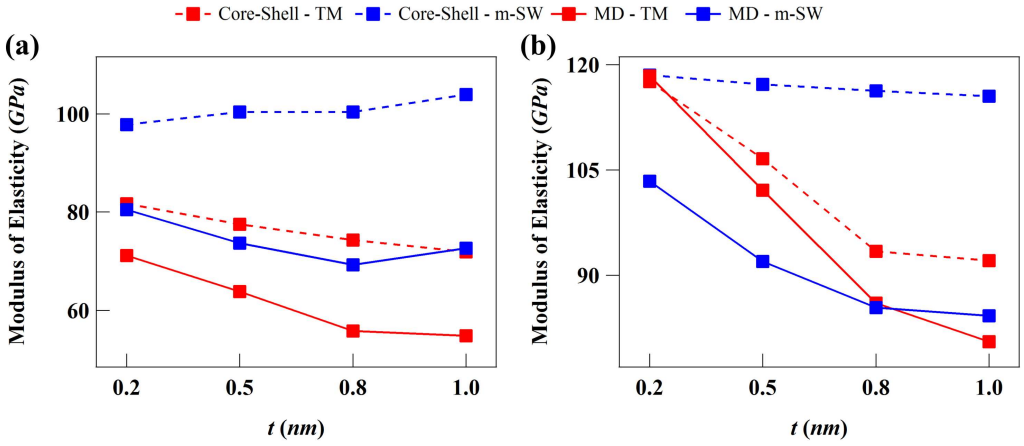

Figure 4: The modulus of elasticity predicted based on the core-shell model and MD simulations for $aSiO_2$-Si NWs of core Si thickness of 4 nm and AR = 20 along (a) $< 100 >$ and (b) $< 110 >$ as a function of the native oxide thickness, t. Results demonstrate and compare the level of success in modulus of elasticity estimation for $aSiO_2$-Si via analytical and MD methods with combined effects native oxide thickness, interatomic potential, and crystalline orientation of Si.

AR of Si NWs, while the size effect on the ultimate strength is negligible for $aSiO_2$-Si NWs. This is in agreement with previous studies, where the impact of oxide layer on the ultimate strength of Si NWs covered with amorphous silica was demonstrated as a reduction from 25 GPa to 8 GPa [46]. Results obtained here for Si NWs can be compared with previous MD simulations. For instance, elastic properties in Table 1 are comparable with previous studies on $< 100 >$ Si NWs with estimations ranging from 40 GPa up to 125 GPa depending on the NW size, interatomic potential and thermodynamic state such as temperature [21, 25, 18, 28]. Similarly, modulus of elasticity values reported for $< 110 >$ Si NWs [29, 20, 25, 18, 19, 23, 22] are comparable with results presented in Table 1 ranging between 60 GPa to 170 GPa. Parameters such as cross-section, AR, temperature, and the interatomic potential cause such a wide range of prediction for modulus of elasticity of Si NWs of different orientations.

After studying the elastic and strength properties, the native oxide effect on the fracture behavior is examined next. Previous studies report different fracture properties in Si NWs, where a range of ductile, brittle or a mixture of both were observed among MD models using different potentials such as the Tersoff-T3, SW and modified Embedded Atom Method (MEAM) potentials

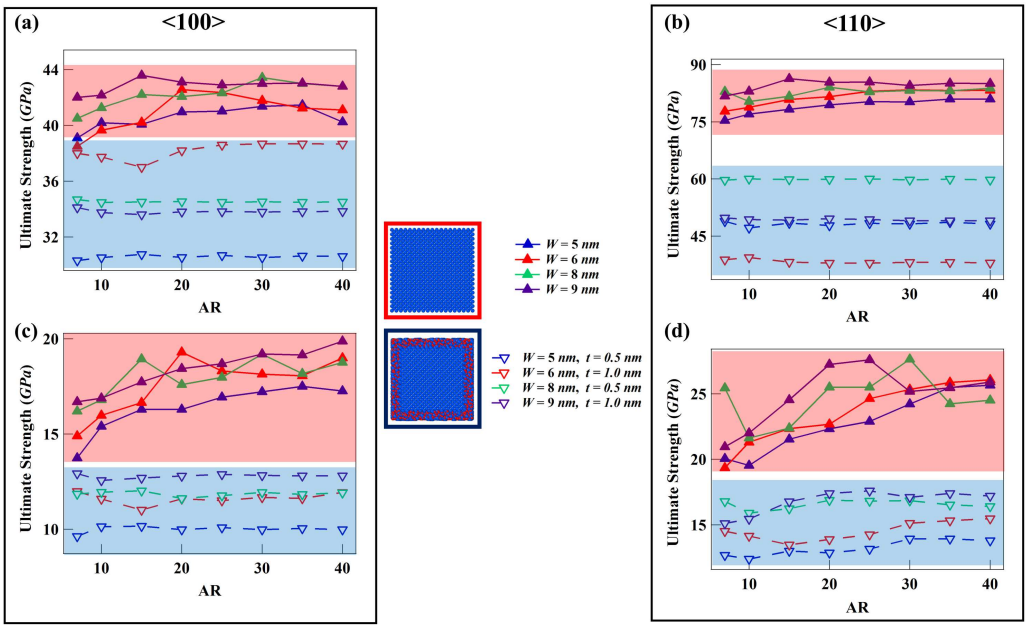

Figure 5: The ultimate strength as a function of AR for Si NWs and $aSiO_2$-Si NWs along (a) $< 100 >$ and (b) $< 110 >$ crystal orientations modeled by the TM potential and along (c) $< 100 >$ and (d) $< 110 >$ crystal orientations modeled by the m-SW potential. Different widths (and different native oxide thicknesses for $aSiO_2$-Si NWs) of NWs are examined where Si NWs and $aSiO_2$-Si NWs are color-coded with red and blue color codes on ultimate strength vs. AR graphs with different levels of reduction due to combined effects of size, native oxide thickness, crystalline orientation, and interatomic potential effects.

[29, 22, 21, 20, 23, 46]. To distinguish the brittle fracture from the ductile behavior, various parameters are recommended as ductility measures by various studies focusing on fracture of NWs [29, 22]. The ductility parameter suggested by Kang and Cai [29] combines the effect of ideal tensile strength and ideal shear strength with Schmid factor predicting a ductile fracture behavior for the Tersoff and SW potentials and reporting brittle fracture modes mostly for the MEAM potentials. In contrast, Xu and Kim [22] introduced a definition to quantify the slip deformation due to the development of cleavage surfaces on (110) plane and {111} plane family, while the brittle fracture in Si NWs were reported similar to the findings of the ductility parameter model [29], confirming a consistent brittle behavior.

To quantify the ductile/brittle failure, a parameter denoted as the ductile failure probability (p) was introduced considering complete brittle and complete ductile failure for $p = 0$ and $p = 1$, respectively [22]. The definition of this parameter is based on the type of fracture categorized as full and partial failures due to necking and slip or cleavage in above mentioned planar directions. The ductile failure parameter is defined as $p = (W_0 - W_{fail})/W_0$, where W_0 is the nominal width and W_{fail} is the width at the failure as shown in Figure 6(a). The criterion for the full necking case is taken as $p > p_{cr} = 0.5$ as suggested previously [22], where the NW remains connected even after the width reduces to less than a half of the nominal value. For all NWs studied in this work, ductile fracture was consistently observed as expected from the TM and m-SW potentials, an observation in parallel with previous findings [29, 20, 31]. Similar ductile fracture was observed for aSiO_2-Si NWs as shown in Figure 6(b) demonstrating full necking during failure. Initiation of the partial reduction in W is represented in left snapshots of Figure 6(a) and Figure 6(b). W is reduced to less than a half of its nominal value due to the full necking while both parts remain connected as shown in the right snapshots of respective figures.

Some partial necking behavior was also observed in aSiO_2-Si NWs while most of NWs failed due to a full necking. Ductile failure probability calculations were performed on NWs represented in Figure 5 and AR = 20. Results in Figure 6(c) show a reduction in the ductile probability with increasing W, indicating an increased probability of ductile fracture with reduced W in both crystal orientations modeled by TM and m-SW potentials. The reduction in ductile failure probability with increasing W as depicted in Figure 6(c) agrees well with previous reports on ductility of Si NWs using Tersoff or MEAM-based interatomic potentials [29, 22]. Moreover, Figure 6(c) also ex-

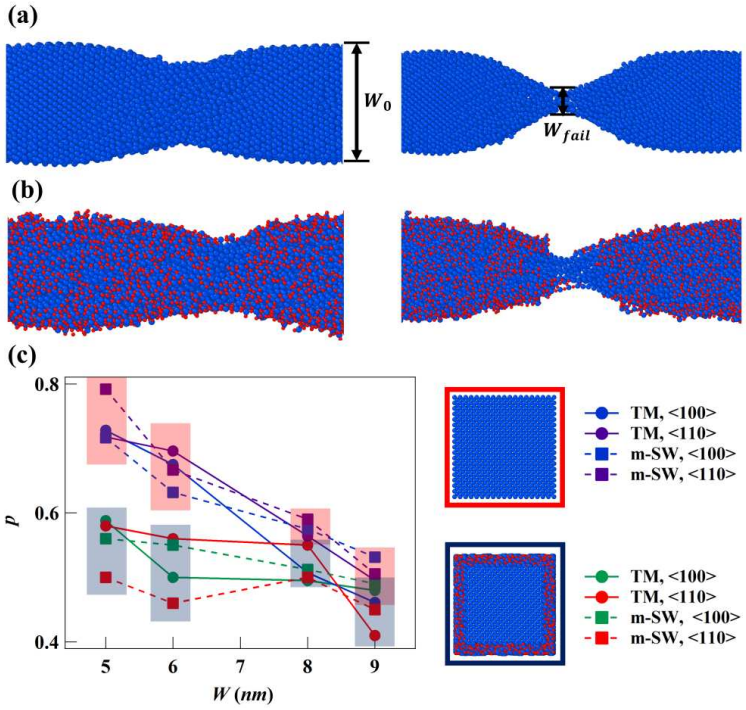

Figure 6: Full necking failure of NWs in (a) Si NW, and (b) $aSiO_2$-Si NW (Blue spheres represent Si and red spheres denote O atoms) where the nominal width (W_0) shown in left images and width at failure (W_{fail}) of the NWs are used for ductile failure probability calculations. (c) Ductile failure probability of Si NWs and $aSiO_2$-Si NWs with associated failure probability estimations color-coded for Si NWs with and without native oxide in red and blue, respectively. The ductile failure probability calculations are conducted for different width of NWs while examining both crystalline orientations ($<$ 100 $>$-Si and $<$ 110 $>$-Si) and both interatomic potentials (TM and m-SW) studied in this work.

hibits ductile failure estimation for $aSiO_2$-Si NWs NWs via both interatomic potentials. The deviations obtained for failure predictions of $aSiO_2$-Si NWs NWs are associated with crystallographic orientation, critical dimension, and oxide layer thickness effects. Hence, ductile failure mechanisms can be captured in Si NWs with a native oxide surface using two common interatomic potentials for Si-O interactions, namely Tersoff and SW. A similar change in the fracture behavior was reported previously for Si NWs [20, 22]. Failure analysis also shows an insignificant dependence of ductile failure probability on NW orientation. Two leading parameters in such a probability analysis are strain rate and temperature, while previous studies demonstrated slightly

less ductile behavior at lower strain rates and lower temperatures [29, 22, 46]. This work utilized a moderate strain rate which is more suitable for tensile simulation of NWs at low temperatures below 10 K for the minimization of the kinetic effects. As a result, a higher size-dependent failure probability for aSiO_2-Si NWs is obtained with a W of 5 nm and 6 nm compared to W of 8 nm and 9 nm as depicted in Figure 6(c). Similarly, previous works on the failure behavior of Si NWs with amorphous silica layer show that NWs with thinner oxide layers fail by necking, while increasing the oxide thickness leads to brittle fracture of Si NWs [46]. Calculating p for aSiO_2-Si NWs at different temperatures can be helpful for the examination of the brittle-to-ductile transition temperature in Si NWs [22, 29].

4. Conclusion

This work investigates the effect of native oxide on the size-dependent mechanical behavior of Si NWs. For this purpose, mechanical properties of pure Si NWs and aSiO_2-Si NWs are compared using MD simulations with TM and m-SW interatomic potentials. The uniaxial tensile deformation is imposed with a strain rate of $\dot{\epsilon} = 5\times10^9 s^{-1}$ at temperatures below 10 K while using periodic B.C.s along the NW length and applying fixed B.C.s along the other two axes. The effect of critical factors such as crystal orientation, oxide thickness, interatomic potential, and AR are examined. The following set of conclusions can be made:

• Both interatomic potentials are found to be reliable for modeling the modulus of elasticity of Si NWs and aSiO_2-Si NWs. On the other hand, the m-SW potential is found to estimate the ultimate strength comparable to previous theoretical and experimental findings. In contrast, the TM potential overestimates the ultimate strength, which can be linked to the soft cut-off scheme in the Tersoff potential.

• Furthermore, the core-shell model is used to verify the impact of native oxide on the size-dependent elastic behavior of Si NWs.

• Results demonstrate an insignificant size effect on the elastic behavior of Si NWs for both crystal orientations, while the native oxide layer reduces the modulus of elasticity considerably with increasing oxide thickness. Similarly, the ultimate strength of aSiO_2-Si NWs is found to be drastically lower than that of Si NWs due to the presence of native oxide. Moreover, the ultimate strength estimations exhibit a negligible AR effect for Si NWs and aSiO_2-Si NWs.

• The reduction in the modulus of elasticity can be as significant as 42%, while strength is observed to diminish by 21%. Such significant reductions in mechanical properties of Si NWs are clear indications of the size effect particularly elaborated as core Si size and native oxide thickness for $aSiO_2$-Si NWs in this study.

• To quantify the failure behavior of $aSiO_2$-Si NWs, ductile failure probability is calculated with mixed behavior observed with full necking failure as the most dominant fracture condition. With decreasing NW width, a higher probability of ductile fracture is observed in Si NWs compared to $aSiO_2$-Si NWs.

•The significant variations in properties and failure mode of Si NWs compared to those exhibited by $aSiO_2$-Si NWs verifies the extremely important and useful outcome of including the native oxide in the interpretation of size dependence of Si NW properties.

• Finally, the contribution of native oxide should be assessed further via combining computational and experimental efforts to examine the physical mechanisms behind size-dependent mechanical behavior of Si NWs.

In fact, various studies considered Si NW surface as a significant factor contributing to mechanical properties including failure mechanisms. However, the present study clearly reveals the important role played by the native oxide layer on the size-dependent mechanical behavior of Si NWs. By doing so, it also sheds further light on the background of various conflicting reports in the literature such as opposing trends of modulus of elasticity estimations with reduced size scale. The findings can serve as a powerful tool for interpretation of size-dependency in properties of Si NWs, as – to the best of our knowledge – no previous MD study exists for inspection of size-dependent properties in Si NWs with native oxide surface condition. The reductions observed in Si NW modulus of elasticity and strength due to the presence of native oxide heavily depend on the thickness of oxide layer. With the probability of ductile failure fracture reduced for Si NWs and $aSiO_2$-Si NWs with increasing W, further study on the prediction of the critical dimension for the initiation of brittle fracture is suggested. Methods such as ideal shear strength calculation of Ref. [29] can be used for this purpose. This is a very valuable insight for the interpretation of experimental observations and extraction of properties from measured data. Elimination of assumptions such as pure Si surface instead of native oxide will further help reduce both the discrepancies between computational and experimental findings and the resulting scatter in estimated modulus of elasticity and fracture strength of

Si NWs. Overall, the present study highlights the importance of native oxide layer on the size-dependent mechanical behavior of Si NWs shedding further light on the background of various conflicting reports in the literature. This work can be extended by incorporating a detailed analysis of the interface between the crystalline Si core and native oxide as well as an examination of further – such as thermal – properties of Si NWs.

Data Availability Statement

The data that support the findings of this study are available from the corresponding author upon reasonable request.

Conflict of Interest

The authors have no conflicts to disclose.

Acknowledgments

S.Z.P. and B.E.A. gratefully acknowledge financial support by Tubitak under grant no 120E347.

References

[1] B. E. Alaca, M. Karimzadehkhouei, Piezoresistive nanowire-based electromechanical sensors, in: Reference Module in Biomedical Sciences, Elsevier, 2021. doi:10.1016/B978-0-12-822548-6.00075-3.

[2] S. Wang, Z. Shan, H. Huang, The Mechanical Properties of Nanowires, Advanced Science 4 (4) (2017) 1–24. doi:10.1002/advs.201600332.

[3] M. M. Rojo, O. C. Calero, A. F. Lopeandia, J. Rodriguez-Viejo, M. Martín-Gonzalez, Review on measurement techniques of transport properties of nanowires, Nanoscale 5 (23) (2013) 11526–11544. doi:10.1039/c3nr03242f.

[4] M. Nasr Esfahani, B. E. Alaca, A Review on Size-Dependent Mechanical Properties of Nanowires, Advanced Engineering Materials 1900192 (2019) 1–23. doi:10.1002/adem.201900192.

[5] Y. Zhu, Mechanics of crystalline nanowires: an experimental perspective, Applied Mechanics Reviews 69 (1) (2017). doi:10.1115/1.4035511.

[6] N. P. Dasgupta, J. Sun, C. Liu, S. Brittman, S. C. Andrews, J. Lim, H. Gao, R. Yan, P. Yang, 25th anniversary article: semiconductor nanowires–synthesis, characterization, and applications, Advanced materials 26 (14) (2014) 2137–2184. doi:10.1002/adma.201305929.

[7] Y. Guerfi, G. Larrieu, Vertical silicon nanowire field effect transistors with nanoscale gate-all-around, Nanoscale research letters 11 (1) (2016) 1–7. doi:10.1186/s11671-016-1396-7.

[8] D. Sacchetto, M. H. Ben-Jamaa, G. De Micheli, Y. Leblebici, Fabrication and characterization of vertically stacked gate-all-around si nanowire fet arrays, in: 2009 Proceedings of the European Solid State Device Research Conference, IEEE, 2009, pp. 245–248. doi:10.1109/ESSDERC.2009.5331516.

[9] T. Sannicolo, M. Lagrange, A. Cabos, C. Celle, J.-P. Simonato, D. Bellet, Metallic nanowire-based transparent electrodes for next generation flexible devices: a review, Small 12 (44) (2016) 6052–6075. doi:10.1002/smll.201602581.

[10] E. Sage, M. Sansa, S. Fostner, M. Defoort, M. Gély, A. K. Naik, R. Morel, L. Duraffourg, M. L. Roukes, T. Alava, et al., Single-particle mass spectrometry with arrays of frequency-addressed nanomechanical resonators, Nature communications 9 (1) (2018) 1–8. doi:10.1038/s41467-018-05783-4.

[11] K. Ekinci, M. Roukes, Nanoelectromechanical systems, Review of scientific instruments 76 (6) (2005) 061101. doi:10.1063/1.1927327.

[12] J. Zhu, X. Liu, Q. Shi, T. He, Z. Sun, X. Guo, W. Liu, O. B. Sulaiman, B. Dong, C. Lee, Development trends and perspectives of future sensors and mems/nems, Micromachines 11 (1) (2020) 7. doi:10.3390/mi11010007.

[13] Y. Kilinc, M. Ç. Karakan, Y. Leblebici, M. S. Hanay, B. E. Alaca, Observation of coupled mechanical resonance modes within suspended

3d nanowire arrays, Nanoscale 12 (43) (2020) 22042–22048. doi:10.1039/D0NR06659A.

[14] T. Miani, T. Verdot, A. Berthelot, F. Maspero, A. Koumela, P. Robert, G. Langfelder, J. Arcamone, M. Sansa, Resonant accelerometers based on nanomechanical piezoresistive transduction, in: 2021 IEEE 34th International Conference on Micro Electro Mechanical Systems (MEMS), IEEE, 2021, pp. 192–195. doi:10.1109/MEMS51782.2021.9375287.

[15] F. W. DelRio, R. F. Cook, B. L. Boyce, Fracture strength of micro-and nano-scale silicon components, Applied Physics Reviews 2 (2) (2015) 021303. doi:10.1063/1.4919540.

[16] M. Elhebeary, M. T. A. Saif, Lessons learned from nanoscale specimens tested by mems-based apparatus, Journal of Physics D: Applied Physics 50 (24) (2017) 243001. doi:10.1088/1361-6463/aa6e2b.

[17] S. Zare Pakzad, M. Nasr Esfahani, Z. Tasdemir, N. Wollschlaeger, X. Li, T. Li, M. Yilmaz, Y. Leblebici, B. E. Alaca, A new characterization approach to study the mechanical behavior of silicon nanowires, MRS Advances (2021) 1–6doi:10.1557/s43580-021-00117-x.

[18] Y. Jing, Q. Meng, W. Zhao, Molecular dynamics simulations of the tensile and melting behaviours of silicon nanowires, Physica E: Low-Dimensional Systems and Nanostructures 41 (4) (2009) 685–689. doi:10.1016/j.physe.2008.11.006.

[19] Y. Jing, Q. Meng, W. Zhao, Atomistic simulations of the tensile and melting behavior of silicon nanowires, Journal of Semiconductors 30 (6) (2009). doi:10.1088/1674-4926/30/6/062003.

[20] K. Kang, W. Cai, Size and temperature effects on the fracture mechanisms of silicon nanowires: Molecular dynamics simulations, International Journal of Plasticity 26 (9) (2010) 1387–1401. doi:10.1016/j.ijplas.2010.02.001.

[21] Q. Liu, S. Shen, On the large-strain plasticity of silicon nanowires: Effects of axial orientation and surface, International Journal of Plasticity 38 (2012) 146–158. doi:10.1016/j.ijplas.2012.05.008.

[22] W. Xu, W. K. Kim, Molecular dynamics simulation of the uniaxial tensile test of silicon nanowires using the meam potential, Mechanics of Materials 137 (May) (2019) 103140. doi:10.1016/j.mechmat.2019.103140.

[23] W. Xu, W. K. Kim, Role of boundary conditions and thermostats in the uniaxial tensile loading of silicon nanowires, Computational Materials Science 178 (February) (2020) 109636. doi:10.1016/j.commatsci.2020.109636.

[24] J. F. Justo, R. D. Menezes, L. V. C. Assali, Stability and plasticity of silicon nanowires: The role of wire perimeter, Physical Review B 75 (4) (2007) 045303. doi:10.1103/PhysRevB.75.045303.

[25] Q. Liu, L. Wang, S. Shen, Effects of geometry and shape on the mechanical behaviors of silicon nanowires, Computers, Materials and Continua 46 (2) (2015) 105–123. doi:10.3970/cmc.2015.046.105.

[26] Z. Yang, Z. Lu, Y. P. Zhao, Shape effects on the yield stress and deformation of silicon nanowires: A molecular dynamics simulation, Journal of Applied Physics 106 (2) (2009). doi:10.1063/1.3186619.

[27] M. N. Esfahani, B. E. Alaca, Surface Stress Effect on Silicon Nanowire Mechanical Behavior: Size and Orientation Dependence, Mechanics of Materials 127 (2018) 112–123. doi:10.1016/j.mechmat.2018.09.004.

[28] X. R. Zhuo, H. G. Beom, Effect of side surface orientation on the mechanical properties of silicon nanowires: A molecular dynamics study, Crystals 9 (2) (2019). doi:10.3390/cryst9020102.

[29] K. Kang, W. Cai, Brittle and ductile fracture of semiconductor nanowires - molecular dynamics simulations, Philosophical Magazine 87 (14-15) (2007) 2169–2189. doi:10.1080/14786430701222739.

[30] Y. Jing, Q. Meng, Molecular dynamics simulations of the mechanical properties of crystalline/amorphous silicon core/shell nanowires, Physica B: Condensed Matter 405 (10) (2010) 2413–2417. doi:10.1016/j.physb.2010.02.056.

[31] J. Godet, F. A. El Nabi, S. Brochard, L. Pizzagalli, Surface effects on the mechanical behavior of silicon nanowires: Consequence on the brittle

to ductile transition at low scale and low temperature, Physica Status Solidi (A) Applications and Materials Science 212 (8) (2015) 1643–1648. doi:10.1002/pssa.201500001.

[32] J. Guénolé, J. Godet, S. Brochard, Deformation of silicon nanowires studied by molecular dynamics simulations, Modelling and Simulation in Materials Science and Engineering 19 (7) (2011). doi:10.1088/0965-0393/19/7/074003.

[33] H. Yao, G. Yun, N. Bai, J. Li, Surface elasticity effect on the size-dependent elastic property of nanowires, Journal of Applied Physics 111 (8) (2012) 083506. doi:10.1063/1.3703671.

[34] J. Chen, J. Shi, Y. Wang, J. Sun, J. Han, K. Sun, L. Fang, Nanoindentation and deformation behaviors of silicon covered with amorphous sio 2: a molecular dynamic study, RSC advances 8 (23) (2018) 12597–12607. doi:10.1039/C7RA13638B.

[35] H. G. Steinrück, A. Schiener, T. Schindler, J. Will, A. Magerl, O. Konovalov, G. Li Destri, O. H. Seeck, M. Mezger, J. Haddad, M. Deutsch, A. Checco, B. M. Ocko, Nanoscale structure of Si/SiO2/organics interfaces, ACS Nano 8 (12) (2014) 12676–12681. doi:10.1021/nn5056223.

[36] T. Watanabe, K. Tatsumura, I. Ohdomari, SiO2/Si interface structure and its formation studied by large-scale molecular dynamics simulation, Applied Surface Science 237 (1-4) (2004) 125–133. doi:10.1016/j.apsusc.2004.06.044.

[37] A. H. Al-Bayati, K. G. Orrman-Rossiter, J. Van Den Berg, D. Armour, Composition and structure of the native si oxide by high depth resolution medium energy ion scatering, Surface science 241 (1-2) (1991) 91–102. doi:10.1016/0039-6028(91)90214-D.

[38] M. Morita, T. Ohmi, E. Hasegawa, M. Kawakami, M. Ohwada, Growth of native oxide on a silicon surface, Journal of Applied Physics 68 (3) (1990) 1272–1281. doi:10.1063/1.347181.

[39] H.-G. Steinruck, A. Schiener, T. Schindler, J. Will, A. Magerl, O. Konovalov, G. Li Destri, O. H. Seeck, M. Mezger, J. Haddad, et al., Nanoscale structure of si/sio2/organics interfaces, ACS nano 8 (12) (2014) 12676–12681. doi:10.1021/nn5056223.

[40] E. H. Poindexter, P. J. Caplan, B. E. Deal, R. R. Razouk, Interface states and electron spin resonance centers in thermally oxidized (111) and (100) silicon wafers, Journal of Applied Physics 52 (2) (1981) 879–884. doi:10.1063/1.328771.

[41] M. T. McDowell, S. W. Lee, I. Ryu, H. Wu, W. D. Nix, J. W. Choi, Y. Cui, Novel size and surface oxide effects in silicon nanowires as lithium battery anodes, Nano Letters 11 (9) (2011) 4018–4025. doi:10.1021/nl202630n.

[42] A. Baumer, M. Stutzmann, M. Brandt, F. Au, S. Lee, Paramagnetic defects of silicon nanowires, Applied physics letters 85 (6) (2004) 943–945. doi:10.1063/1.1775288.

[43] J. Chen, J. Shi, Y. Wang, J. Sun, J. Han, K. Sun, L. Fang, Nanoindentation and deformation behaviors of silicon covered with amorphous sio 2: a molecular dynamic study, RSC advances 8 (23) (2018) 12597–12607. doi:10.1039/C7RA13638B.

[44] H. Sadeghian, C. Yang, J. Goosen, E. Van Der Drift, A. Bossche, P. French, F. Van Keulen, Characterizing size-dependent effective elastic modulus of silicon nanocantilevers using electrostatic pull-in instability, Applied Physics Letters 94 (22) (2009) 221903. doi:10.1063/1.3148774.

[45] H. Sadeghian, C.-K. Yang, J. F. Goosen, A. Bossche, U. Staufer, P. J. French, F. van Keulen, Effects of size and defects on the elasticity of silicon nanocantilevers, Journal of Micromechanics and Microengineering 20 (6) (2010) 064012. doi:10.1088/0960-1317/20/6/064012.

[46] W. Xu, Molecular dynamics simulations of the size-dependent brittle-to-ductile transition of silicon nanowires, Ph.D. thesis, University of Cincinnati (2020).

[47] Y. He, G. Galli, Microscopic origin of the reduced thermal conductivity of silicon nanowires, Physical review letters 108 (21) (2012) 215901. doi:10.1103/PhysRevLett.108.215901.

[48] X. Zhou, J. Hu, C. Li, D. Ma, C. Lee, S. Lee, Silicon nanowires as chemical sensors, Chemical Physics Letters 369 (1-2) (2003) 220–224. doi:10.1016/S0009-2614(02)02008-0.

[49] A. Ilinov, A. Kuronen, Atomistic modeling of bending properties of oxidized silicon nanowires, Journal of Applied Physics 115 (10) (2014) 104305. doi:10.1063/1.4868318.

[50] H. Ohta, T. Watanabe, I. Ohdomari, Strain distribution around sio2/si interface in si nanowires: A molecular dynamics study, Japanese journal of applied physics 46 (5S) (2007) 3277. doi:10.1143/JJAP.46.3277.

[51] S. Z. Pakzad, M. N. Esfahani, B. E. Alaca, Molecular dynamics study of orientation-dependent tensile properties of si nanowires with native oxide: Surface stress and surface energy effects, in: 2021 IEEE 21st International Conference on Nanotechnology (NANO), IEEE, 2021, pp. 370–373. doi:10.1109/NANO51122.2021.9514301.

[52] H. S. Park, Surface stress effects on the resonant properties of silicon nanowires, Journal of Applied Physics 103 (12) (2008) 123504. doi:10.1063/1.2939576.

[53] S. Munetoh, T. Motooka, K. Moriguchi, A. Shintani, Interatomic potential for Si-O systems using Tersoff parameterization, Computational Materials Science 39 (2) (2007) 334–339. doi:10.1016/j.commatsci.2006.06.010.

[54] T. Watanabe, I. Ohdomari, Modeling of SiO2/Si(100) interface structure by using extended -Stillinger-Weber potential, Thin Solid Films 343-344 (1-2) (1999) 370–373. doi:10.1016/S0040-6090(98)01700-3.

[55] T. Watanabe, H. Fujiwara, H. Noguchi, T. Hoshino, I. Ohdomari, Novel Interatomic Potential Energy Function for Si, O Mixed Systems, Japanese Journal of Applied Physics, Part 1: Regular Papers and Short Notes and Review Papers 38 (4 PART 2) (1999) 366–369. doi:10.1143/jjap.38.l366.

[56] P. Ganster, G. Treglia, A. Saul, Atomistic modeling of strain and diffusion at the si/sio 2 interface, Physical Review B 81 (4) (2010) 045315. doi:10.1103/PhysRevB.81.045315.

[57] P. Vashishta, R. K. Kalia, J. P. Rino, I. Ebbsjö, Interaction potential for sio 2: A molecular-dynamics study of structural correlations, Physical Review B 41 (17) (1990) 12197. doi:10.1103/PhysRevB.41.12197.

[58] X. R. Zhuo, H. G. Beom, Atomistic study of the bending properties of silicon nanowires, Computational Materials Science 152 (May) (2018) 331–336. doi:10.1016/j.commatsci.2018.06.009.

[59] F. Östlund, K. Rzepiejewska-Malyska, K. Leifer, L. M. Hale, Y. Tang, R. Ballarini, W. W. Gerberich, J. Michler, Brittle-to-ductile transition in uniaxial compression of silicon pillars at room temperature, Advanced Functional Materials 19 (15) (2009) 2439–2444. doi:10.1002/adfm.200900418.

[60] J. Godet, P. Hirel, S. Brochard, L. Pizzagalli, Evidence of two plastic regimes controlled by dislocation nucleation in silicon nanostructures, Journal of Applied Physics 105 (2) (2009) 108–111. doi:10.1063/1.3072707.

[61] X. Han, K. Zheng, Y. Zhang, X. Zhang, Z. Zhang, Z. L. Wang, Low-temperature in situ large-strain plasticity of silicon nanowires, Advanced Materials 19 (16) (2007) 2112–2118. doi:10.1002/adma.200602705.

[62] S. Huang, S. Zhang, T. Belytschko, S. S. Terdalkar, T. Zhu, Mechanics of nanocrack: Fracture, dislocation emission, and amorphization, Journal of the Mechanics and Physics of Solids 57 (5) (2009) 840–850. doi:10.1016/j.jmps.2009.01.006.

[63] D.-M. Tang, C.-L. Ren, M.-S. Wang, X. Wei, N. Kawamoto, C. Liu, Y. Bando, M. Mitome, N. Fukata, D. Golberg, Mechanical properties of si nanowires as revealed by in situ transmission electron microscopy and molecular dynamics simulations, Nano letters 12 (4) (2012) 1898–1904. doi:10.1021/nl204282y.

[64] S. Plimpton, Fast parallel algorithms for short-range molecular dynamics, Journal of computational physics 117 (1) (1995) 1–19. doi:10.1006/jcph.1995.1039.

[65] J. Cormier, J. M. Rickman, T. J. Delph, Erratum: Stress calculation in atomistic simulations of perfect and imperfect solids (J. Appl. Phys. (2001) 89 (99)), Journal of Applied Physics 89 (7) (2001) 4198. doi:10.1063/1.1354656.

[66] F. Xu, Q. Qin, A. Mishra, Y. Gu, Y. Zhu, Mechanical properties of Zno Nanowires under different loading modes, Nano Research 3 (4) (2010) 271–280. doi:10.1007/s12274-010-1030-4.

[67] C. Q. Chen, Y. Shi, Y. S. Zhang, J. Zhu, Y. J. Yan, Size dependence of young's modulus in zno nanowires, Physical review letters 96 (7) (2006) 075505. doi:10.1103/PhysRevLett.96.075505.

[68] M.-Q. Le, D.-T. Nguyen, Atomistic simulations of pristine and defective hexagonal bn and sic sheets under uniaxial tension, Materials Science and Engineering: A 615 (2014) 481–488. doi:10.1016/j.msea.2014.07.109.

[69] M. N. Esfahani, Comparing empirical interatomic potentials to modeling silicon surface stress, Solid State Communications 344 (2022) 114656. doi:10.1016/j.ssc.2022.114656.

[70] T. Belytschko, S. Xiao, G. Schatz, R. Ruoff, Atomistic simulations of nanotube fracture, Physical Review B 65 (23) (2002) 235430. doi:10.1103/PhysRevB.65.235430.

[71] M.-Q. Le, D.-T. Nguyen, The role of defects in the tensile properties of silicene, Applied Physics A 118 (4) (2015) 1437–1445. doi:10.1007/s00339-014-8904-3.

[72] D. Shir, B. Liu, A. Mohammad, K. Lew, S. Mohney, Oxidation of silicon nanowires, Journal of Vacuum Science & Technology B: Microelectronics and Nanometer Structures Processing, Measurement, and Phenomena 24 (3) (2006) 1333–1336. doi:10.1116/1.2198847.

[73] H. Ohta, T. Watanabe, I. Ohdomari, Strain distribution around SiO2/Si interface in Si nano wires: A molecular dynamics study, Japanese Journal of Applied Physics, Part 1: Regular Papers and Short Notes and Review Papers 46 (5 B) (2007) 3277–3282. doi:10.1143/JJAP.46.3277.

[74] S. H. Park, J. S. Kim, J. H. Park, J. S. Lee, Y. K. Choi, O. M. Kwon, Molecular dynamics study on size-dependent elastic properties of silicon nanocantilevers, Thin Solid Films 492 (1-2) (2005) 285–289. doi:10.1016/j.tsf.2005.06.056.

[75] J. J. Wortman, R. A. Evans, Young's modulus, shear modulus, and poisson's ratio in silicon and germanium, Journal of Applied Physics 36 (1) (1965) 153–156. doi:10.1063/1.1713863.

[76] H. Ni, X. Li, H. Gao, Elastic modulus of amorphous SiO 2 nanowires, Applied Physics Letters 88 (4) (2006) 1–3. doi:10.1063/1.2165275.

[77] H. Scholze, Glass: nature, structure, and properties, Springer Science & Business Media, 1991. doi:10.1007/978-1-4613-9069-5.

[78] E. C. Silva, L. Tong, S. Yip, K. J. Van Vliet, Size effects on the stiffness of silica nanowires, Small 2 (2) (2006) 239–243. doi:10.1002/smll.200500311.

[79] L. P. Dávila, V. J. Leppert, E. M. Bringa, The mechanical behavior and nanostructure of silica nanowires via simulations, Scripta Materialia 60 (10) (2009) 843–846. doi:10.1016/j.scriptamat.2008.12.057.

[80] F. Yuan, L. Huang, Molecular dynamics simulation of amorphous silica under uniaxial tension: From bulk to nanowire, Journal of Non-Crystalline Solids 358 (24) (2012) 3481–3487. doi:10.1016/j.jnoncrysol.2012.05.045.

[81] F. Yuan, L. Huang, Size-dependent elasticity of amorphous silica nanowire: A molecular dynamics study, Applied Physics Letters 103 (20) (2013) 201905. doi:10.1063/1.4830038.

[82] X.-J. Xu, Y.-C. Wang, B. Wang, K. Zhang, A modified size-dependent core–shell model and its application in the wave propagation of square cellular networks, Physica E: Low-dimensional Systems and Nanostructures 80 (2016) 53–61. doi:10.1016/j.physe.2016.01.005.

[83] M. Nasr Esfahani, S. Zare Pakzad, T. Li, X. Li, Z. Tasdemir, N. Wollschlager, Y. Leblebici, B. E. Alaca, Effect of native oxide on stress in silicon nanowires: Implications for nanoelectromechanical systems, ACS Applied Nano Materials (2022). doi:10.1021/acsanm.2c02983.

[84] A. P. Bartók, J. Kermode, N. Bernstein, G. Csányi, Machine learning a general-purpose interatomic potential for silicon, Physical Review X 8 (4) (2018) 041048. doi:10.1103/PhysRevX.8.041048.